Sensors & Diagnostics

PAPER

View Article Online
View Journal | View Issue

Cite this: *Sens. Diagn.*, 2023, **2**, 721

Noninvasive and point-of-care screening of snoring by breath monitoring using ion-in-conjugation polymer-based humidity sensors†

Ze-Kun Chen,[a] Wei-Wei Bai,[a] Ying-Qian Huo*[b] and Jing-Hui He *[a]

Received 17th February 2023,
Accepted 9th April 2023

DOI: 10.1039/d3sd00042g

rsc.li/sensors

Snoring monitoring is a valid method to assess human health. However, it is challenging to sense the humidity of breath flows that have huge oscillations, requiring highly robust sensors. Herein, a humidity sensor based on ion-in-conjugation croconate polymers was fabricated for snoring monitoring for the first time. The sensor showed rapid response/recovery to monitor human breathing. It has a wide working range from 11% to 95% RH (relative humidity) with a time stability of up to 28 800 seconds (8 hours). Normal breath, snoring, and apnea are distinguished and recorded timely. The fabricated noninvasive and point-of-care snoring detection device exhibits comparable accuracy to commercial devices, manifesting the potential of ion-in-conjugation polymers in future breath monitoring systems.

1. Introduction

Snoring can cause nocturnal hypoxemia and apnea increasing the incidence of cardiovascular and cerebrovascular diseases.[1] Screening the respiration signal is a point-of-care method to evaluate the health of the human body, especially if snoring and apnea occur during sleep.[2] Previous snoring monitors considered several acoustical indexes, such as sound pressure level, sound energy, and percentage snoring time.[3] Since one of the main constituents of exhaled gas is water molecules, the humidity of exhaled gas varies with the intensity and rate of breathing. Hence, applying humidity sensors with ultratime stability to sensing snoring is feasible. Humidity sensors capable of screening the status of breath should meet some critical criteria, such as rapid response time,[16b] low values of humidity hysteresis, and most importantly, robustness towards the respiration flows of the huge oscillations of humidity.[4–10]

The performance of humidity sensors relies on the working principle and sensing materials being applied, such as two-dimensional materials,[11] polymers,[12] and ceramics.[13] Among them, conjugated polymers have attracted increasing attention due to their structural diversity, tunability, controllable performance, and low cost.[14] However, many conjugated polymers suffer from long-time instability and low sensitivity to humidity.[15] Recently, ion-in-conjugation polymers, containing ionic states in the conjugated backbones, were investigated owing to their unparalleled physical and chemical properties.[16a] Our previous work has shown that ion-in-conjugation polymers have strong affinity to polar molecules, including water, because of highly polar ionic fragments, rendering breath monitoring viable.[16b] In addition, the strong inter-molecular interactions and good crystallinity of ion-in-conjugation polymers can resist the corrosion of water vapor and provide good robustness for humidity sensing. Humidity sensors were prepared from two polycroconate materials: poly(1,5-diaminoanthraquinone-croconate) (1,5-PDAC) and poly(2,6-diaminoanthraquinone-croconate) (2,6-PDAC).

In this study, we demonstrate for the first time that ion-in-conjugation polymers can be utilized for snoring monitoring and breath apnea, comparable to commercial apparatuses (Fig. 1). As a proof of concept of ion-in-conjugation polymers, two polycroconates were prepared, which showed impedance

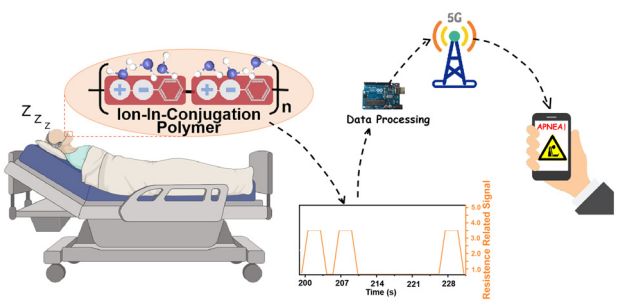

Fig. 1 Illustration of the noninvasive and point-of-care screening of snoring.

[a] *Suzhou Key Laboratory of Novel Semiconductor-Optoelectronics Materials and Devices, College of Chemistry, Chemical Engineering and Materials Science, Soochow University, Suzhou 215123, P.R. China. E-mail: jinghhe@suda.edu.cn*
[b] *Department of Neurology, Binzhou Medical University Hospital, Binzhou, Shandong Province, 256603, P.R. China. E-mail: yqhuo_BMU@126.com*

† Electronic supplementary information (ESI) available. See DOI: https://doi.org/10.1039/d3sd00042g

ranging from 10^4 to 10^8 Ω, the time of response and recovery within seconds and the humidity hysteresis less than 6% toward the atmosphere of relative humidity from 11% to 95%. Normal breath and snoring were successfully distinguished and recorded remotely using ion-conjugated-polymer-based resistive sensors to monitor the humidity of exhaled gas from nostril outlets with a time stability of up to 28 800 s. The noninvasive and point-of-care snoring detection device is comparable to the accuracy of commercial devices, indicating the potential commercial application of ion-in-conjugation polymers in future screening snoring and apnea systems based on humidity.

2. Results and discussion

2.1. Material and characterizations

The ion-on-conjugation polymers and polycroconates were prepared by condensing croconic acids with 1,5-diaminoanthraquinone (1,5-DAAQ) and 2,6-diaminoanthraquinone (2,6-DAAQ). The Fourier-Transform Infrared (FT-IR) spectra were used to characterize the successful synthesis of the product structures (Fig. 2a). The disappearance of $-NH_2$ at 3421 cm^{-1} and 3319 cm^{-1} in 1,5-DAAQ, and –OH at 3482 cm^{-1} in croconic acid, indicated the successful polycondensation between 1,5-DAAQ and croconic acid. The formation of an *ortho*-position polymer between 1,5-DAAQ and croconate is due to the characteristic peaks of carbonyls (C═O) at 1795 cm^{-1} and 1723 cm^{-1} in Fig. 2b.[17,18] Identically, 2,6-PDAC was synthesized through polycondensation in the *para*-position, as shown in Fig. 2c. 1,5-PDAC shows relatively regular microcrystals (Fig. 2d) with diameters of approximately 50 nm and 2,6-PDAC displays the morphology of a loose structure (Fig. 2f). Fig. 2e and g are TEM images of 1,5-PDAC and 2,6-PDAC. The elemental mapping graphics of the two polymers showed that the elements were evenly distributed (Fig. S1 and S2†).

Furthermore, it can be seen from X-ray diffraction (XRD) data that 1,5-PDAC has better crystallinity than 2,6-PDAC in Fig. S3a,† possibly due to the strong double hydrogen bond interaction provided by ion-conjugated polymers.[19] In terms of electronic properties, the Tauc plots show that the energy gaps (E_g) of 1,5-PDAC and 2,6-PDAC, shown in Fig. S3b,† are 1.44 eV and 1.57 eV, respectively, which means that their properties of semiconducting are appropriate for humidity sensing. In terms of thermal stability, we compared the weight loss of the polymers at 200 °C in a nitrogen environment to exclude the influence of material hygroscopicity. The above-mentioned results indicate that 1,5-PDAC has better thermostability than 2,6-PDAC (Fig. S4a and b†). 1,5-PDAC shows a smaller specific surface area than 2,6-PDAC (Fig. S5a and b†) calculated using the Brunauer–Emmett–Teller (BET). These properties prove that the two polymers are suitable for humidity sensing.

2.2. Humidity sensing properties

The polymer powder was brush-coated onto interdigitated electrodes to fabricate a resistive sensor, which was placed in a chamber with different relative humidities and connected to an external impedance analyzer (Fig. S6†). The operating frequency will affect the performance of humidity sensors.[16a] Exploring the optimal frequency of humidity sensing by varying the frequencies from 20 Hz to 1 MHz to measure different impedance values under different RHs at 25 °C (Fig. 3). Generally, the impedance decreases with the increase of humidity at a certain frequency, and the impedance decreases with increasing work frequency at a fixed RH. In Fig. 3a, the impedance values of the humidity sensor based

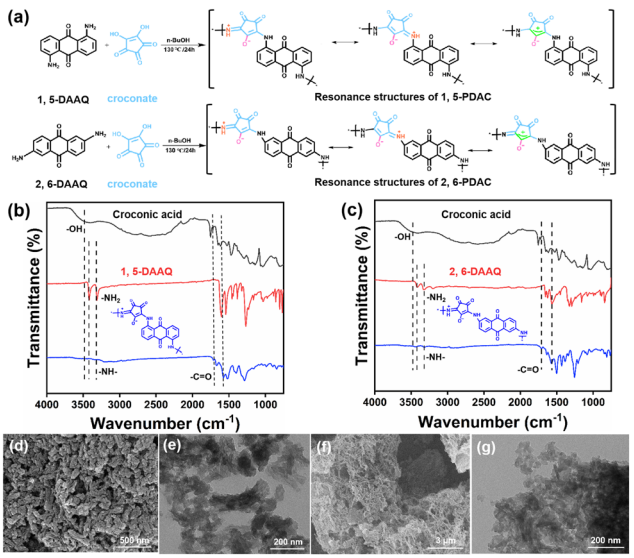

Fig. 2 (a) The synthesis roadmaps and resonance structures of 1,5-PDAC, and 2,6-PDAC. The FT-IR spectra of (b) 1,5-PDAC with its relevant reagents and (c) 2,6-PDAC with its reagents. (d) SEM and (e) TEM images of 1,5-PDAC. (f) SEM and (g) TEM images of 2,6-PDAC.

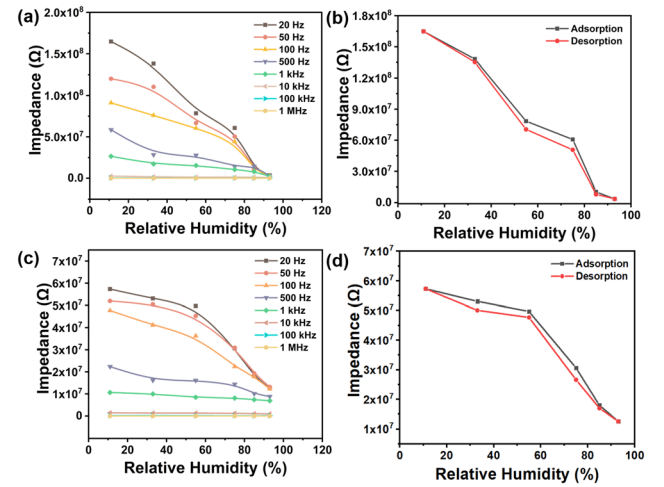

Fig. 3 Impedance change at different RHs for humidity sensors based on (a) 1,5-PDAC and (c) 2,6-PDAC ranging from 20 Hz to 1 MHz. The humidity hysteresis of humidity sensors based on (b) 1,5-PDAC and (d) 2,6-PDAC at 20 Hz.

on 1,5-PDAC vary linearly with humidity change. The impedance of the humidity sensor based on 2,6-PDAC changed logarithmically at low RH (less than 54%) and linearly at high RH (Fig. 3c). Furthermore, the impedance of the two polymer-based humidity sensors decreased significantly with the increase of frequency under humidity below 54%. This phenomenon indicates that the impedance value is greatly affected by the operating frequency under the humidity condition of less than 54%. Frequency has nearly no effect on impedance, although there is a slight change in impedance as frequency increases under high humidity conditions. We finally chose the test conditions of 20 Hz and 1 V because of the broad impedance range from 10^4 to 10^8 Ω.

As one of the most important indexes to evaluate the reliability of humidity sensors, humidity hysteresis is defined as the maximum RH difference at the identical impedance modulus on the curve when the sensor experiences humidity moisture adsorption and desorption.[20] Humidity hysteresis is caused by the higher impedance of the adsorption process due to the higher exothermic adsorption rate than the endothermic desorption rate[16a] (calculation details are shown in Fig. S7†). In Fig. 3b and d, the humidity hysteresis of 1,5-PDAC and 2,6-PDAC is 6.4% and 9%, respectively.

In terms of humidity sensor sensitivity, the response time (t_{res}, time when the response change reaches 90% of the maximum signal) and recovery time (t_{rec}, time when the response drop change reaches 90% of the steady response) are other significant characteristics for breath monitoring. We made several pulses at 11% RH and 95% RH at 20 Hz, as shown in Fig. S8a and d† to obtain the t_{res} and t_{rec} of 1,5-PDAC, and 2,6-PDAC-based humidity sensors, respectively. The t_{res} of the 2,6-PDAC sensor is 120 s when switching from 11% to 95% RH in Fig. S8b,† and the t_{rec} is approximately 10 s, as shown in Fig. S8c.† In contrast, the t_{res} of the 1,5-PDAC sensor is short enough (10 s) to have the potential to track human breathing (Fig. S8e and f†). Compared with the reported polymer materials, the t_{res} of 1,5-PDAC is short enough to successfully monitor human breathing, which is superior to many other sensory materials.[21–23] In summary, the humidity sensor based on 1,5-PDAC can operate over a broad range of RH, and the time stability of 1,5-PDAC up to 28 800 seconds (8 hours) also lays the foundation for its application in the field of screening snoring and apnea (Fig. S9†).

2.3. Humidity sensing mechanism

We explored the humidity sensing mechanism *via* impedance spectra,[20–23] which were collected on 1,5-PDAC and 2,6-PDAC at 1 V with different operating frequencies under different humidity conditions. Both the real part ReZ and the imaginary part-ImZ are amplified simultaneously in complex impedance spectra to facilitate the comparison.

The humidity sensing properties of 1,5-PDAC are the strongest among these two polymers. The complex impedance spectra of 1,5-PDAC, as shown in Fig. 4a, indicate

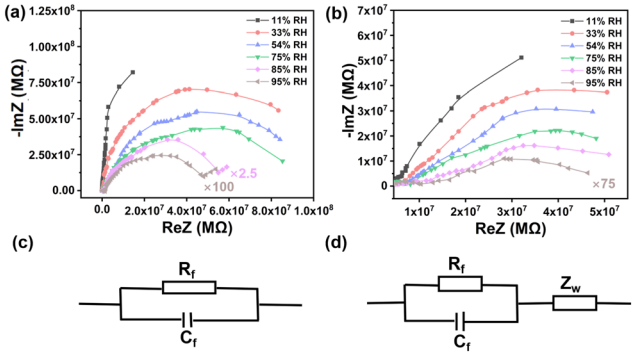

Fig. 4 Complex impedance plots of a humidity sensor based (a) 1,5-PDAC and (b) 2,6-PDAC. (c and d) The electric equivalent circuits.

that the arc radius is larger at low humidity (11–33% RH), while the arc gradually becomes a semicircle with increasing humidity. The equivalent circuit of the complex impedance spectra of 1,5-PDAC is formed by a resistor (R_f) and a condenser (C_f) in parallel[24,25] (Fig. 4c). As the humidity increases to 95%, the radius of the semicircle decreases, the straight line followed becomes longer, and the equivalent circuit becomes a Warburg impedance (Z_w)[26] series connection with resistors and capacitors in parallel (Fig. 4d). The Warburg impedance results from the diffusion of charge carriers between the hygrosensitive material and the electrode interface. At low humidity, a small number of water molecules are physically adsorbed on the hygrosensitive material surface in the form of hydrogen bonds. Therefore, physically adsorbed water molecules are unable to move freely, resulting in difficulties in ionic conduction. The equivalent circuit shown in Fig. 4c confirms the above logic. With the gradual increase in humidity, the number of physically adsorbed water molecules increases to form multiple layers of water. The movement of ions in the continuous water layer is mainly from H^+ and H_3O^+, which are formed by the ionization of H^+ and transferred through the Grotthuss chain reaction ($H_2O + H_3O^+ \rightarrow H_3O^+ + H_2O$),[27] resulting in the decrease of impedance with the equivalent circuit in Fig. 4d. Similarly, the complex impedance plot of 2,6-PDAC indicates the same characteristics as 1,5-PDAC in Fig. 4b. Compared with 2,6-PDAC, the spectral radius of 1,5-PDAC shrinks faster, and the straight line becomes longer, indicating that 1,5-PDAC has the strongest adsorption capacity among these two polymers.

2.4. Application in screening human breathing snoring

Inspired by the super sensitivity of 1,5-PDAC, we designed a noninvasive and point-of-care moisture analysis system to detect the snoring of a volunteer as shown in Fig. 5a. The snoring monitoring system consists of our humidity sensor, a headphone-adapted holder to fix the humidity sensor, a circuit board to receive, process, and transmit the humidity signals, Arduino and a mobile phone or computer installing real-time analysis software to remotely

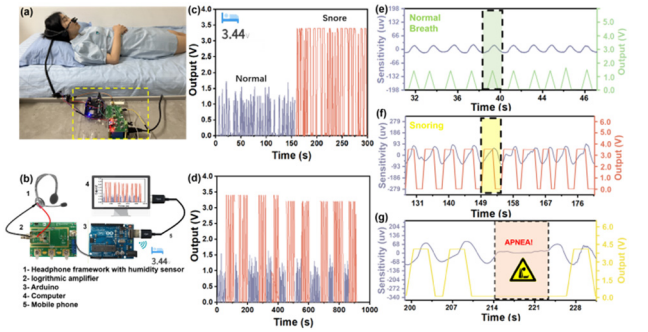

Fig. 5 (a) Sketch of breath snore monitoring; (b) schematic diagram of breath monitoring based on the 1,5-PDAC humidity sensor; (c) human breath test in two different modes; (d) sensor cycle stability test; (e) real-time monitoring of normal breathing (the blue line is the commercial detector, the green line is the point-of-care sensor and the magnified illustration in Fig. S10a†); (f) real-time monitoring of snoring (the blue line is the commercial detector, the red line is the point-of-care sensor and the magnified illustration in Fig. S10b†); (g) real-time monitoring of apnea in the process of snoring.

monitor the snoring (Fig. 5b). The circuit board with a signal converter converted the humidity oscillation into electrical signals, which the Arduino gathered and disposed of in real-time and exported the voltage signal. Finally, the database was conveyed to the application on a mobile phone or computer by 5G modules.[28–30] Although the temperature will affect the absolute water vapor pressure and consequently modulate the sensor signal, the breath monitoring function is unaffected because we only collect the changes of electrical signals caused by obvious humidity fluctuations, rather than exact humidity values. The noninvasive and point-of-care snoring sensors provide a source of inspiration for further commercial development in human sleeping health monitoring.

A volunteer wore a headphone and breathed in two different models (snoring and normal). The interdigital electrode covered by the polymers is placed 1 cm away from her nostril outlet without the need for an invasion into her nostril. In the breath monitoring test, the 1,5-PDAC-based humidity sensor was integrated into the headphone under ambient conditions, with the RH of exhaled and inhaled gas ranging from 11% to 95%. The results showed that under such an RH range, the humidity sensor can synchronously respond and recover with breath regardless of different breath modes, indicating that the sensor has the ability to capture the rate of human breath and ensure the utility of the device (Fig. 5c). After converting the impedance to analogue voltage (0–4 V), the signal is transmitted to a computer or mobile phone for facile remote monitoring. Compared to normal breathing, the further increase in the output signal during snoring is due to the higher humidity during deep breathing, resulting in a lower impedance of the humidity sensor. Therefore, normal breathing and snoring can be distinguished (Fig. 5c). To explore its potential application, we further tested the circulatory stability of the above-mentioned breath sensors (Fig. 5d). The device can accurately distinguish snoring and normal breath modes, indicating the potential for respiratory health detection.

We compared the data with a commercial snoring detector (EEG-1200C from Nihon Kohden Corp) to demonstrate the sensitivity and commercial potential of our noninvasive and point-of-care sensor. To realize synchronous monitoring using the commercial detector and our sensors, we first reduced the sampling frequency to 1 Hz to allow long-term operation. The commercial detector was tested using invasive methods that fix the detector inside the nasal cavity. In contrast, our sensors used a noninvasive method for point-of-care snoring detection. A volunteer wore the commercial monitor and our noninvasive sensor at the same time (Fig. S11†) to synchronize the output of sensitivity and voltage signal of real-time breathing data. Initially, during the normal breathing period, our noninvasive sensor had the same sensitivity as the commercial detectors, and the signal fluctuated in line with breathing (Fig. 5e). As snoring occurs, slower breathing (Fig. S9a and b†) presents a plateau in the data of our sensor, comparable and synchronal to the plateau of the commercial detector (Fig. 5f). Furthermore, the disappearance of data fluctuations for more than 10 seconds, belonging to apnea, will cause an alarm remotely through 5G or Bluetooth transmission (Fig. 5g). With these functions, the sensor has great commercial potential for point-of-care detection of the snoring process and apnea.

Conclusion

In summary, two ion-in-conjugation polymers, polycroconates, were synthesized and applied in the screening of snoring. 1,5-PDAC-based humidity sensors showed excellent performance: response/recovery time within seconds in a wide humidity range (11–95%), a time stability of up to 28 800 seconds (8 hours), and a maximum humidity hysteresis of less than 6%. Normal breath, snoring, and apnea are distinguished and recorded timely. Furthermore, the noninvasive and point-of-care snoring detection devices are comparable to the accuracy of commercial devices. Our results demonstrated that ion-in-conjugation polymers have promising commercial applications for snoring detection.

Author contributions

Ze-Kun Chen: writing-original draft, investigation. Wei-Wei Bai: software. Ying-Qian Huo: investigation, formal analysis, resources, writing-review, and editing. Jing-Hui He: conceptualization, supervision, funding acquisition, writing-review, and editing. All authors have given approval to the final version of the manuscript.

Conflicts of interest

There are no conflicts to declare.

Acknowledgements

The authors gratefully acknowledge the financial support provided by the National Natural Science Foundation of China (21978185), the Suzhou Science and Technology Bureau Project (SYG201935), and the project supported by the Priority Academic Program Development of Jiangsu Higher Education Institutions (PAPD).

Notes and references

1 Z. Li, Q. Song, L. Cheng and M. Tan, *Sci. China Inf. Sci.*, 2021, **64**, 174201.
2 R. E. Davis, G. R. McGregor and K. B. Enfield, *Environ. Res.*, 2016, **144**, 106–116.
3 R. Fischer, T. S. Kuehnel, V. Vielsmeier, F. Haubner, S. Mueller and C. Rohrmeier, *Eur. Arch. Otorhinolaryngol.*, 2020, **277**, 1227–1233.
4 J. Dai, H. Zhao, X. Lin, S. Liu, Y. Liu, X. Liu, T. Fei and T. Zhang, *ACS Appl. Mater. Interfaces*, 2019, **11**, 6483–6490.
5 Z. Yang, L. Guo, B. Zu, Y. Guo, T. Xu and X. Dou, *Adv. Opt. Mater.*, 2014, **2**, 738–745.
6 B. Zu, B. Lu, Z. Yang, Y. Guo, X. Dou and T. Xu, *J. Phys. Chem. C*, 2014, **118**, 14703–14710.
7 S. Sainio, T. Palomäki, S. Rhode, M. Kauppila, O. Pitkänen, T. Selkälä, G. Toth, M. Moram, K. Kordas, J. Koskinen and T. Laurila, *Sens. Actuators, B*, 2015, **211**, 177–186.
8 S. Wang, Z. Chen, A. Umar, Y. Wang, T. Tian, Y. Shang, Y. Fan, Q. Qi and D. Xu, *J. Phys. Chem. C*, 2015, **119**, 28640–28647.
9 J.-F. Lin, J. Kukkola, T. Sipola, D. Raut, A. Samikannu, J.-P. Mikkola, M. Mohl, G. Toth, W.-F. Su, T. Laurila and K. Kordas, *J. Mater. Chem. A*, 2015, **3**, 4687–4694.
10 Z. Yang, A. Liu, C. Wang, F. Liu, J. He, S. Li, J. Wang, R. You, X. Yan, P. Sun, Y. Duan and G. Lu, *ACS Sens.*, 2019, **4**, 1261–1269.
11 N. T. Hue, Q. Wu, W. Liu, X. Bu, H. Wu, C. Wang, X. Li and X. Wang, *Nanotechnology*, 2021, **32**, 115501.
12 L. Wang, J. Xu, X. Wang, Z. Cheng and J. Xu, *Sens. Actuators, B*, 2019, **288**, 289–297.
13 M. Anbia, S. E. Moosavi Fard, K. Shafiei, M. A. Hassanzadeh and A. Mayahipour, *Chin. J. Chem.*, 2012, **30**, 842–846.
14 D.-S. Han and M.-S. Gong, *Sens. Actuators, B*, 2010, **145**, 254–258.
15 H. Zhao, X. Lin, R. Qi, J. Dai, S. Liu, T. Fei and T. Zhang, *IEEE Sens. J.*, 2019, **19**, 833–837.
16 (*a*) C. Yu, J.-H. He and J.-M. Lu, *Small*, 2022, e2204023, DOI: **10.1002/smll.202204023**; (*b*) X. Xiao, Q.-J. Zhang, J.-H. He, Q.-F. Xu, H. Li, N.-J. Li, D.-Y. Chen and J.-M. Lu, *Sens. Actuators, B*, 2018, **255**, 1147–1152.
17 J. Zhou, X.-F. Cheng, B.-J. Gao, C. Yu, J.-H. He, Q.-F. Xu, H. Li, N.-J. Li, D.-Y. Chen and J.-M. Lu, *Small*, 2019, **15**, 1803896.
18 J. Zhou, H. Lin, X.-F. Cheng, J. Shu, J.-H. He, H. Li, Q.-F. Xu, N.-J. Li, D.-Y. Chen and J.-M. Lu, *Mater. Horiz.*, 2019, **6**, 554–562.
19 P. Clément, S. Korom, C. Struzzi, E. J. Parra, C. Bittencourt, P. Ballester and E. Llobet, *Adv. Funct. Mater.*, 2015, **25**, 4011–4020.
20 W. Dong, Z. Ma and Q. Duan, *Sens. Actuators, B*, 2018, **272**, 14–20.
21 D. Qi, C. Zhao, Z. Zhuang, G. Li and H. Na, *Electrochim. Acta*, 2016, **197**, 39–49.
22 C. Ru, Y. Gu, Z. Li, Y. Duan, Z. Zhuang, H. Na and C. Zhao, *J. Electroanal. Chem.*, 2019, **833**, 418–426.
23 H. Zhao, T. Zhang, R. Qi, J. Dai, S. Liu, T. Fei and G. Lu, *Sens. Actuators, B*, 2017, **248**, 803–811.
24 R. Hao, X. Xiao, X. Zuo, J. Nan and W. Zhang, *J. Hazard. Mater.*, 2012, **209–210**, 137–145.
25 Z. Chen, Y. Wang, Y. Shang, A. Umar, P. Xie, Q. Qi and G. Zhou, *Sci. Rep.*, 2017, **7**, 2713.
26 W. Geng, Q. Yuan, X. Jiang, J. Tu, L. Duan, J. Gu and Q. Zhang, *Sens. Actuators, B*, 2012, **174**, 513–520.
27 S. Heidari, M. Haghighi and M. Shabani, *Ultrason. Sonochem.*, 2018, **43**, 61–72.
28 J. Yang, R. Shi, Z. Lou, R. Chai, K. Jiang and G. Shen, *Small*, 2019, **15**, 1902801.
29 Q. Cao, C. Yu, X.-F. Cheng, W.-J. Sun, J.-H. He, N.-J. Li, H. Li, D.-Y. Chen, Q.-F. Xu and J.-M. Lu, *Sens. Actuators, B*, 2020, **320**, 128390.
30 Z.-S. Zhang, J.-X. Liu, X.-F. Cheng, J.-H. He, H. Li, Q.-F. Xu, N.-J. Li, D.-Y. Chen and J.-M. Lu, *Sens. Actuators, B*, 2021, **330**, 129353.